IEEE Access
Multidisciplinary | Rapid Review | Open Access Journal

Received June 14, 2017, accepted June 22, 2017, date of publication June 27, 2017, date of current version July 24, 2017.

Digital Object Identifier 10.1109/ACCESS.2017.2720465

An Image-Based Hair Modeling and Dynamic Simulation Method

YONGTANG BAO[1] AND YUE QI[1,2], (Member, IEEE)
[1]State Key Laboratory of Virtual Reality Technology and Systems, Beihang University, Beijing 100191, China
[2]Beihang University Qingdao Research Institute, Qingdao 266100, China

Corresponding author: Yue Qi (qy@buaa.edu.cn)

This work was supported in part by the National Natural Science Foundation of China under Grant 61572054 and in part by the Applied Basic Research Program of Qingdao under Grant 16-10-1-3-xx.

ABSTRACT In the past years, significant progress has been made in image-based hair modeling, thus producing abundant 3-D hair models. However, on the one hand, the reconstructed hair models could not preserve the structural details of hairstyle. On the other hand, there exists little research on these modeling results. Currently, hair geometry is mostly represented as mass chains of 3-D points. It is difficult to simulate hair directly from this representation. In this paper, we propose a novel approach to convert hair geometry model into helices, which could be easily plugged into dynamic hair simulation. We construct a hair model from a hybrid orientation field, which is generated from four fields. We extract a representative guide hair strand model from this hair geometry. Then, we use adaptive floating tangents fitting algorithm to convert this hair geometry into a physics-based hair model. To initialize this hair model, we calculate a corresponding static equilibrium configuration under external forces, including gravity, frictional contacts, and viscous drag from ambient air. We simulate dynamic hair by the Euler–Lagrange equations. Our approach can preserve structural details of 3-D hair models, and can be applied to simulate various hair geometries.

INDEX TERMS Image-based hair modeling, hybrid orientation field, adaptive floating tangents fitting, dynamic hair simulation.

I. INTRODUCTION

Realistic 3D hair models and motions of hair are very important in various applications due to their contributions for fidelity of virtual characters. Hair modeling and dynamic simulation are all research focuses in the field of computer graphics. Currently, one way to reconstruct a hair model is physics-based hair modeling. But it is really hard to generate a desired hair model since there are too many parameters in these physical models. Another way to reconstruct a hair model is image-based hair modeling. This method can achieve higher quality with lower effort. However, on the one hand, prior image-based hair modeling methods cannot guarantee the reconstructed hair models preserving the structural details. On the other hand, there exists little research on these hair modeling results, especially on hair simulation from a reconstructed hairstyle. These two areas of research have not been connected from each other.

Most of the image-based hair modeling methods have typically reconstructed hair models by orientation field [1], [2]. These approaches can reconstruct hair models with interior real distribution, but the exterior hair strands are not similar to the images. Most of the image-based hair modeling results are represented as mass chains of 3D points. This representation of hair cannot be used for dynamic simulation. In traditional super-helix model [3], hair is represented as piecewise helices which can be used for hair simulation.

The goal of our work is to convert the reconstructed realistic hair geometry model into a physics-based hair model and simulate hair features. Our technique achieves this by combining three components: a realistic hair model reconstructed using hybrid orientation field, a physics-based hair model generated by adaptive floating tangents fitting algorithm, and a dynamic hair simulation method that can verify the effectiveness of our method. We reconstruct a realistic hair model from a hybrid orientation field, which is generated from multiple fields. Next, we convert the hair geometry model into physics-based hair model. Each hair strand is approximated with G^1 piecewise helices by adaptive floating tangents fitting algorithm. These helices could be easily pugged into dynamic hair simulation. Finally, we initialize the parameters of hair simulation and simulate dynamic hair by Euler-Lagrange equations. We show that our converted

physics-based hair models can be used to simulate dynamic hair features.

In summary, our main contributions are:

- An novel approach for hair simulation from captured input images. A hybrid orientation field is firstly constructed from the input images. Then a reconstructed hair model is generated from this hybrid orientation field by combining the interior real distribution and the exterior structural details. Finally, this realistic hair geometry model is converted into a physics-based hair model. Hair features are simulated from this physics-based model.
- An effective adaptive floating tangents fitting algorithm. It can approximate a hair strand with G^1 piecewise helices. Parameters of these helices can be computed by this algorithm.
- A new framework for hair simulation. We construct an Euler-Lagrange dynamic equation using accurate expression of energy and calculate a corresponding static equilibrium configuration under external forces.

II. RELATED WORK

Over the past years, realistic hair synthesis has drawn the interest of computer scientists [4]. We briefly review the image-based hair modeling and simulation in the following categories.

A. IMAGE-BASED HAIR MODELING

Recently, some researchers proposed 3D hair modeling methods from multiple hair images [1], [2], [5]. They generated an orientation field from images based on triangulation and traced hair strands from this field. With thermal imaging techniques, Herrera *et al.* [6] reconstructed a high-quality hair model by sidestepping anisotropic hair reflectance and complicated segmentation among skin and hair. Beeler *et al.* [7] introduced a system to reconstruct sparse facial hair and skin simultaneously, which could deliver the best result in the presence of short, sparse hair. Luo *et al.* [8] reconstructed complex hairstyles with plausible hair structure. This method could preserve structure-aware details, but it only reconstructed the surface of hair models. Xu *et al.* [9] proposed a dynamic hair modeling method, which utilized the motion path analysis and solved space-time consistency to produce realistically dynamic hair models both in geometry and motion details. Yu *et al.* [10] presented a hybrid image-CAD based system, which could reconstruct many hairstyles.

In addition to hair modeling from multiple images, there have been a lot of single-view hair modeling researches recently. Bonneel *et al.* [11] estimated plausible hair appearance and geometry from a single photo rather than faithful reconstruction. Chai *et al.* [12] demonstrated a single view hair modeling for manipulation on portrait images. Echevarria *et al.* [13] generated a printable 3D surface with stylized color and geometric details, but they could not reconstruct highly-detailed individual hair strands. Hu *et al.* [14] proposed a single-view hair modeling method based on their hairstyle database. Chai *et al.* [15] reconstructed high-quality hair models from a single portrait photo based on shading, silhouettes and a helical prior. But this method could not process frizzy hairstyles because of ambiguous silhouettes. More recently, Chai *et al.* [16] presents an automatic hair modeling from a single image.

B. PHYSICS-BASED HAIR SIMULATION

While early methods [17], [18] focused on animating individual hair strands without taking into account hair mutual interactions, most recent techniques [3], [19] have attempted to capture real-word strand behaviors. Based on these models, methods [19]–[21] that operate on the strand level and take into account complex hair interactions can yield high-fidelity results. Recently, many researches [22], [23] use the discrete elastic rod formulation [24] for hair simulation. This elastic rod model has become the current industry standard for hair simulation. Daviet *et al.* [25] developed a hybrid approach that robustly simulate the Coulomb friction effects between hair fibers. Chai et at. [26] presented an adaptive method for interactive hair-solid simulation using a compact strand-based hair skinning model. More recently, Fei *et al.* [27] proposes a novel multi-component simulation framework to simulate Liquid-Hair interactions.

Currently, the limitation of hair simulation is the difficulty to initialize the model accurately with a sample geometry. Some researches have been started already in order to bridge this gap. Hadap [28] and Derouet-Jourdan *et al.* [29] leveraged exact inverse statics for fibers under gravity, but considered only isolated fibers. Twigg and Kačić-Alesić [30] proposed to reduce the sagging effect of hair through nonlinear optimization. Focusing more on the high-performance simulation of hairs, various simplified representations have been proposed to accelerate hair mutual interactions. Hadap and Magnenat-Thalmann [31] applied fluid dynamic models to resolve hair collisions. Bando *et al.* [32] modeled hairs as loosely connected particles that were animated in a continuum way.

III. OVERVIEW

Figure 1 shows the pipeline of our method. Its input is a set of images captured from multiple views around a hairstyle (Figure 2). We key the images automatically using a color classifier trained with a Gaussian Mixture Model [33], and use patch-based multi-view stereo algorithm (PMVS) [34] to reconstruct point cloud with normal (denoted as $\mathcal{P}_c$). We trace *directed 3D strand segments* (denoted as $\mathcal{ST}$) by the approach in [35]. Next, we run following three steps:

(1)Image-based hair modeling (Sect. IV). A hybrid orientation field is generated from four fields which are constructed from *directed 3D strand segments*. Hair strands automatically grow from uniformly distributed hair roots according to the hybrid orientation field.

(2)Adaptive floating tangents fitting (Sect. V). Each representative hair strand is approximated with G^1 piecewise helices. Parameters of these helices are computed by our adaptive floating tangents fitting algorithm. After getting

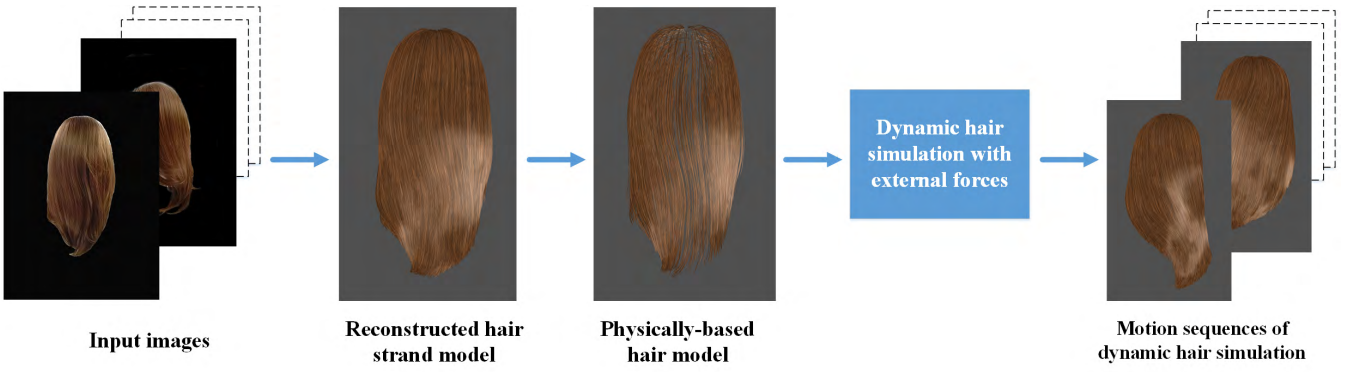

FIGURE 1. The pipeline of our method. We start with a set of captured hair images, reconstruct a hair strand model from a hybrid orientation field, and convert this hair geometry model into physics-based model using adaptive floating tangents fitting algorithm. Finally, a series of hair motion sequence are generated by dynamic hair simulation.

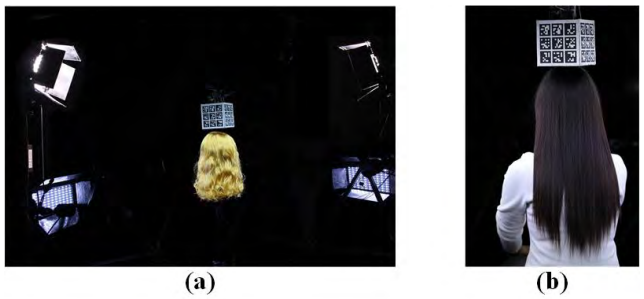

FIGURE 2. Our capture device. (a) capturing wig hairstyle; (b) capturing real hairstyle.

parameterized piecewise helices, we build a static physics-based hair model.

(3)Dynamic hair simulation (Sect. VI). We initialize the parameters of hair simulation by calculating a corresponding static equilibrium configuration under external forces. Then we simulate dynamic hair by Euler-Lagrange equations to verify our method.

IV. IMAGE-BASED HAIR MODELING

We use a hybrid orientation field to construct a hair strand model. This model is represented as mass chains of 3D points.

A. GENERATING A HYBRID ORIENTATION FIELD

Having traced *directed 3D strand segments* $\mathcal{ST}$, we utilize them to generate a hybrid orientation field. The hybrid orientation field (denoted as $\mathbf{H}$) is generated from four fields, including a surface-structure orientation field (denoted as $\mathbf{S}_s$), an interior orientation field (denoted as $\mathbf{V}_i$), an interior distance field (denoted as I_d), and a growing orientation field (denoted as $\mathbf{O}_g$). $\mathbf{S}_s$ makes the surface structure of a hairstyle be similar to the input images. $\mathbf{V}_i$ makes the hair roots and interior hair strands be consistent with actual distribution. The tracing hair strands can be confined to the hair volume according to I_d. $\mathbf{O}_g$ makes the growing direction at a hair strand be compatible with its predecessor. Compared with other prior works, these fields contain not only the interior actual distribution but also the exterior structural details of hair. To generate these four fields, we first calculate a bounding box of hair volume according to the point cloud $\mathcal{P}_c$. We then discretize the bounding box into voxels. The voxel size used in our examples is 2mm.

To generate $\mathbf{V}_i$, we diffuse the direction defined on the $\mathcal{ST}$ and the hair roots. The voxels containing either part of a 3D strand segment or a hair root are considered as known voxels, whose directions are the strand segment's direction or root direction. We use the known voxels as Dirichlet boundary condition to solve a Laplace equation, which is defined as

$$\Delta \mathbf{V} = \frac{\partial^2 \mathbf{V}}{\partial x^2} + \frac{\partial^2 \mathbf{V}}{\partial y^2} + \frac{\partial^2 \mathbf{V}}{\partial z^2} = 0,$$

where $\mathbf{V} = \mathbf{v}\mathbf{v}^T$, $\mathbf{v}$ is the direction in each voxel.

We group the *directed 3D strand segments* $\mathcal{ST}$ into ribbons based on their spatial similarity in local regions. We then choose the ribbons that have compatible growth directions as our *directed hair ribbons*. And lastly, we generate $\mathbf{S}_s$ by diffusing the directions defined on all directed ribbons. The $\mathbf{S}_s$ is computed by reusing the regular grid which is used for $\mathbf{V}_i$ diffusion. The voxels containing part of a ribbon are considered as known voxels whose directions are the ribbon's direction. We solve a Laplace equation to obtain $\mathbf{S}_s$, where the known voxels are set as Dirichlet boundary condition.

To construct I_d, we reuse the 3D regular grid used for the $\mathbf{V}_i$ and $\mathbf{S}_s$ diffusion solve and store I_d there. A voxel that is occupied by a directed 3D strand segment or a head model is considered as a *hair boundary voxel*, in which we store a zero distance-field value. The distance values of the boundary voxels of the bounding box volume is set to the smallest Euclidean distance between that voxel and any hair boundary voxel. The values of all other voxels are computed by a diffusion equation. The growing direction of each voxel in $\mathbf{O}_g$ is determined by the direction of two neighbouring positions in each strand.

We define the hybrid orientation field $\mathbf{H}$ as

$$\mathbf{H} = \alpha_s \mathbf{S}_s + \alpha_i \mathbf{V}_i + \alpha_d \nabla I_d + \alpha_g \mathbf{O}_g, \quad (1)$$

TABLE 1. The differences in generating a hybrid orientation field between our method and realistic hair modeling method [35].

Method	Regular grid	Interior orientation field	Diffusion method	Structure details preserving
Realistic modeling	using $\mathcal{ST}$	using $\mathcal{ST}$ and hair roots normal	by fractional anisotropy	using optimization strategy
Our method	using $\mathcal{P}_c$	using $\mathcal{ST}$ and Laplace equation	by directed ribbons and Laplace equation	using directed ribbons

where $\alpha_s, \alpha_i, \alpha_d$, and α_g are dynamical weights corresponding to each field respectively, ∇ is the gradient value of interior distance field I_d.

This hybrid orientation field is similar to the field in [35]. However, compared with their fractional anisotropy method, we use *directed hair ribbons* to support authentic exterior structure of a hairstyle when we trace hair strands from hair roots since the directed ribbons contain abundant structural details of a hairstyle. Table 1 shows the differences in generating a hybrid orientation field between our method and realistic hair modeling method [35].

B. GENERATING HAIR MODEL

After computing the hybrid orientation field $\mathbf{H}$, we now generate a hair model by growing individual strands from uniformly distributed hair roots. For each new growing point p_i in every strand (denoted as $\mathcal{S}$), its position is computed by Eq. (2):

$$p_i = p_{i-1} + \delta\Big(\mathbf{H}\left(p_{i-1}\right)\Big), \tag{2}$$

where p_{i-1} is the predecessor of p_i on hair strand $\mathcal{S}$, δ is the growing step (1.0mm), $\mathbf{H}\left(p_{i-1}\right)$ is the value of hybrid orientation field computed by Eq. (1) at point p_{i-1}.

We compute the smallest Euclidean distance (denoted as d_s) between p_{i-1} and the *directed ribbons* to determine the dynamical weights in Eq. (1). For each new growing point p_i, the values of α_s, α_i, α_d and α_g in Eq. (1) are determined by d_s following two conditions: (i) If $d_s < T_S$ (T_S is a threshold, $T_S = 0.1$mm), we set $\alpha_s = 100 - d_s$, $\alpha_i = 0.1$, $\alpha_d = 0.1 * \alpha_i$, and $\alpha_g = 10$; (ii) If $d_s \geq T_S$, we set $\alpha_s = 0$, $\alpha_i = 100 * d_s$, $\alpha_d = 0.1 * \alpha_i$, and $\alpha_g = 10$. These two conditions make the new growing point be compatible with the real distribution. If p_{i-1} is closer to the hair surface, the value of α_s is larger, whereas the value of it is smaller until it is zero.

The new point p_i is grown repeatedly until any of the following conditions is met: (i) The new growing point p_i is out of hair volume where $I_d\left(p_i\right) > I_{bound}$; (ii) The growing strand has reached a maximum length. Next, we convert this hair geometry model into physics-based model in Sec. V.

V. ADAPTIVE FLOATING TANGENTS FITTING

To accelerate hair simulation, we extract a reduced hair geometry from the reconstructed hair strand model by hierarchical clustering algorithm. We then convert this reduced hair model into physics-based hair model to simulate hair features. For each hair strand in this reduced hair model, we approximate it with a G^1 piecewise helical curve, which could be described with only three parameters per element and could be easily plugged into dynamic hair simulation. As described in Algorithm 1, we approximate each hair strand with a Bézier spline by the method in [29]. The element number N is derived in Sec. V-A. We adaptively calculate N according to the spline length and curvature. In Sec. V-B, we relax break points to satisfy the interpolation condition. Parameters (curvature, torsion and length) of each helix are calculated in Sec. V-C.

Algorithm 1 Framework of Adaptive Floating Tangents Fitting Algorithm

Input: a reduced model of reconstructed hair strand model.
Output: parameters for each piecewise helical curve.

```
for each hair strand in the hair model do
    Approximate hair strand with a Bézier spline;
    Adaptively calculate the segment number N of spline;
    Cut spline into N pieces and calculate tangents at each break point;
    for each neighboring break points do
        Relax break points to satisfy the interpolation condition;
        Interpolate points and tangents of each subsequent break points;
    end for
end for
```

A. CALCULATING ELEMENT NUMBER

As discussed in [29], the number of helical elements is very important for approximating each hair strand with a G^1 piecewise helical curve. On the one hand, with too small a number of elements on a lengthy hair strand, the piecewise helical curve may not match the input hair strand. On the other hand, approximating a small hair strand with too high a number of elements may yield very close break points. The length of the hair strand is the main influencing factor during approximating hair strand with helical curve. We use N_{min} to N_{max} elements for the hair strand model. Generally, if the length of hair strand L is less than L_{min}, we set $N = N_{min}$. If the length of hair strand L is more than L_{max}, we set $N = N_{max}$. In other cases, we use the Algorithm 2 to calculate an appropriate element number. In this adaptive algorithm, we firstly calculate the median of N_{min} and N_{max} as the initial value of N. We then cut the spline into N pieces and compute a set of tangents at these break points. Finally, we compute the inner product (denote as $\langle \mathbf{t}_i, \mathbf{t}_{i+1} \rangle$) of two

neighboring break points. Its value reflects the complexity of the spline [36].

Algorithm 2 Adaptively Calculating the Element Number

Input: the smallest and biggest element number N_{min} and N_{max}.
Output: an appropriate element number N.

```
Initialization N, N = ⌊(N_min + N_max)/2⌋
Cut the spline into N pieces of same length and compute a set of tangents {t_0, t_1, ..., t_N} at break points;
for each neighboring break points (t_i, t_{i+1}) do
    if ⟨t_i, t_{i+1}⟩ ≤ 0 then
        N = N + 1;
    end if
    if ⟨t_i, t_{i+1}⟩ > 0.95 then
        N = N − 1;
    end if
end for
return N;
```

B. RELAXING BREAK POINTS

1) CO-HELICAL CONDITION

Having calculated the element number in Sec. V-A, we cut the spline into N pieces of same length and compute the tangents at the break points. We now have N+1 points $\{\mathbf{p}_0, \mathbf{p}_1, ..., \mathbf{p}_N\}$, along with their respective tangents $\{\mathbf{t}_0, \mathbf{t}_1, ..., \mathbf{t}_N\}$. The second pass of our method builds N smoothly connected helices by fitting exactly one helix between two successive points.

Given an input spline, we claim that satisfying exactly the tangents $\{\mathbf{t}_0, \mathbf{t}_1, ..., \mathbf{t}_N\}$ is more important than interpolation the positions $\{\mathbf{p}_0, \mathbf{p}_1, ..., \mathbf{p}_N\}$, because this is necessary for preserving the general look of the spline. This problem statement based on the interpolation of *floating tangents* [37] under some neighboring conditions on their new points gives rise to an original scheme for building G^1-smooth piecewise helices. We relax points $\{\mathbf{p}_0, \mathbf{p}_1, ..., \mathbf{p}_N\}$ to unknown positions $\{\mathbf{p}_0^*, \mathbf{p}_1^*, ..., \mathbf{p}_N^*\}$ so that each pair of new points $\mathbf{p}_i^*, \mathbf{p}_{i+1}^*$ along with their tangent vectors $\mathbf{t}_i^*, \mathbf{t}_{i+1}^*$ are co-helical. It means a helix goes through $\mathbf{p}_i^*$ and $\mathbf{p}_{i+1}^*$ with $\mathbf{t}_i^*$ and $\mathbf{t}_{i+1}^*$ as respective tangents - and so that the new tangents $\{\mathbf{t}_0^*, \mathbf{t}_1^*, ..., \mathbf{t}_N^*\}$ match the old ones, that is $\forall i \in \{0, ..., N\}$, $\mathbf{t}_i^* = \mathbf{t}_i$.

Ghosh [37] expressed the co-helical condition, stating that two points $\mathbf{p}_i$ and $\mathbf{p}_{i+1}$ along with their two tangent vectors $\mathbf{t}_i$ and $\mathbf{t}_{i+1}$ are co-helical if and only if

$$\langle \mathbf{p}_{i+1} - \mathbf{p}_i, \mathbf{t}_{i+1} - \mathbf{t}_i \rangle = 0, \tag{3}$$

where $\langle \mathbf{a}, \mathbf{b} \rangle$ denotes the inner product in $\mathbb{R}^3$ between vectors $\mathbf{a}$ and $\mathbf{b}$.

2) APPROXIMATION WITH N HELICES

In the case of N helices, we have N+1 points $\mathcal{P} = \{\mathbf{p}_0, \mathbf{p}_1, ..., \mathbf{p}_N\}$ along with their tangents $\mathcal{T} = \{\mathbf{t}_0, \mathbf{t}_1, ..., \mathbf{t}_N\}$. We relax the points to their new positions $\mathcal{P}^* = \{\mathbf{p}_0^*, \mathbf{p}_1^*, ..., \mathbf{p}_N^*\}$ to make them fulfill the co-helical condition:

$$\forall i \in \{0, ..., N-1\}, \langle \mathbf{p}_{i+1}^* - \mathbf{p}_i^*, \mathbf{t}_{i+1} - \mathbf{t}_i \rangle = 0. \tag{4}$$

Considering $\{\mathbf{t}_0, \mathbf{t}_1, ..., \mathbf{t}_N\}$, we build N matrices

$$\mathbf{D}_i = \begin{pmatrix} \mathbf{v}_{0,i} & \mathbf{v}_{1,i} \end{pmatrix}$$

with $(\mathbf{v}_{0,i}, \mathbf{v}_{1,i})$ a basis of the vectorial plane normal to the vector $\mathbf{t}_{i+1} - \mathbf{t}_i$. Starting from $\mathbf{p}_0^*$, $\forall i \in \{1, ..., N\}$, we get $\mathbf{p}_i^* = \mathbf{p}_0^* + \sum_{j=0}^{i-1} \mathbf{D}_j \mathbf{a}_j$ with $\mathbf{a}_j = \begin{pmatrix} \alpha_{0,j} \\ \alpha_{1,j} \end{pmatrix} \in \mathbb{R}^2$. The constrained minimization problem is described as:

$$\min_{\mathcal{A}, \mathbf{p}_0^*} \sum_{i=1}^{N} \left\| \mathbf{p}_0^* + \sum_{j=0}^{i-1} \mathbf{D}_j \mathbf{a}_j - \mathbf{p}_i \right\|^2 = \min_{\mathcal{A}, \mathbf{p}_0^*} F_{\mathcal{V}, \mathcal{P}}(\mathcal{A}, \mathbf{p}_0^*), \tag{5}$$

with $\mathcal{A} = \{\alpha_{i,0}, \alpha_{i,1} | i \in [0, N-1]\}$ and $\mathcal{V} = \{\mathbf{v}_{i,0}, \mathbf{v}_{i,1} | i \in [0, N-1]\}$. We solve this quadratic problem for $\mathcal{A}$ and $\mathbf{p}_0^*$ using LU decomposition.

C. CALCULATING PARAMETERS

Having computed the co-helical positions and tangents in Sec. V-B, we address the problem of interpolating two points along with two tangents using a single helix. More precisely, we start by describing a helix $\mathbf{r}$ and its tangent $\mathbf{t}$ in an adapted frame. This frame is built from the tangent $\mathbf{t}_0$ at the starting point and from the Darboux vector Ω of the helix. Let $\{\mathbf{t}, \mathbf{n}, \mathbf{b}\}$ be its Frenet frame, which satisfies

$$\begin{pmatrix} \mathbf{t}' \\ \mathbf{n}' \\ \mathbf{b}' \end{pmatrix} = \begin{pmatrix} 0 & k & 0 \\ -k & 0 & \tau \\ 0 & -\tau & 0 \end{pmatrix} \begin{pmatrix} \mathbf{t} \\ \mathbf{n} \\ \mathbf{b} \end{pmatrix}, \tag{6}$$

with k the curvature and τ the torsion along the helix $\mathbf{r}$. We write the Darboux vector as

$$\Omega = \tau \mathbf{t} + k \mathbf{b}, \tag{7}$$

which satisfies $\mathbf{t}' = \Omega \times \mathbf{t}$, $\mathbf{n}' = \Omega \times \mathbf{n}$, $\mathbf{b}' = \Omega \times \mathbf{b}$. A helix $\mathbf{r}$ and its tangent $\mathbf{t}$ can be defined as

$$\begin{aligned} \mathbf{r}(s) &= \mathbf{p}_0 + \bar{\tau} s \bar{\mathbf{\Omega}} + \frac{\sin \omega s}{\omega} (\mathbf{t}_0 - \bar{\tau} \bar{\mathbf{\Omega}}) - \frac{1 - \cos \omega s}{\omega} (\mathbf{t}_0 \times \bar{\mathbf{\Omega}}) \\ \mathbf{t}(s) &= \mathbf{t}_0 + (\cos \omega s - 1)(\mathbf{t}_0 - \bar{\tau} \bar{\mathbf{\Omega}}) - \sin \omega s (\mathbf{t}_0 \times \bar{\mathbf{\Omega}}), \end{aligned} \tag{8}$$

with $\mathbf{p}_0$ the starting point of the helix and $\mathbf{t}_0$ its tangent, ω is the norm of Darboux vector Ω, $\bar{\mathbf{\Omega}}$ is the normalized vector $\bar{\mathbf{\Omega}} = \frac{1}{\omega} \Omega$, and τ its torsion with $\bar{\tau} = \frac{\tau}{\omega}$. The curvature of the helix can be obtained by $k = \sqrt{\omega^2 - \tau^2}$.

After the definition of a helix, we calculate the parameters of it by the interpolation algorithm in [38]. Having calculated the parameters of each helix, we get a physics-based hair model. Next, we will simulate dynamic hair features by this model.

VI. DYNAMIC HAIR SIMULATION

To initialize the parameters of hair simulation, we calculate a corresponding static equilibrium configuration under external forces. In other terms, we consider the *inverse* problem [39] which consists in enforcing the static configuration of hair and retrieving the corresponding physical parameters. In our problem, the generalized coordinate $\mathbf{q}$ (discrete curvatures and torsions) are directly provided by the geometric fitting of the input geometry model. We only need to estimate the intrinsic hair curliness $\mathbf{q}^0$ and the contact forces $\mathbf{F}^c$. In practice, we take $\mathbf{q}^0_{est} = \mathbf{q}$ and search for contact forces $\mathbf{F}^c$ that guarantee an exact equilibrium state for hair while minimizing hair internal elastic energy.

We simulate dynamic hair by Euler-Lagrange equations. Given the generalized coordinate $\mathbf{q}$, the Euler-Lagrange equations of motion can be defined as

$$\frac{d}{dt}\left(\frac{\partial T}{\partial q'_{j,Q}}\right) - \frac{\partial T}{\partial q_{j,Q}} + \frac{\partial V}{\partial q_{j,Q}} + \frac{\partial D}{\partial q'_{j,Q}} = \int_0^L \mathbf{J}_{j,Q} \cdot \mathbf{F} ds, \quad (9)$$

where $\mathbf{J}_{j,Q}$ defines the Jacobian matrix and $\mathbf{J}_{j,Q} = \frac{\partial \mathbf{r}}{\partial q_{j,Q}}$, $q_{j,Q}$ is the j-th curvature of segment Q, (for $j = 0, 1, 2$ *and* $1 \le Q \le N$), $q'_{j,Q}$ is the derivative of $q_{j,Q}$ to t, T is kinetic energy, V is potential energy, D is dissipation energy, $\mathbf{F}$ is the total forces, including gravity, viscous drag and frictional contact:

$$\mathbf{F} = \rho S \mathbf{g} + \mathbf{F}^c - \nu \mathbf{r}', \quad (10)$$

where ρS is the mass of the helix per unit length, $\mathbf{r}' = d\mathbf{r}/dt$ is the derivative of $\mathbf{r}$ to t, $\mathbf{g}$ is the acceleration of gravity, $\mathbf{F}^c$ is the contact forces, ν is the viscous coefficient with the ambient air.

Following, we formulate the three energies in the equations of motion. The kinetic energy T is composed of T_t and T_r. T_t is the translational energy of the centerline $\mathbf{r}$. And T_r is the rotational energy of the rod cross section. The translational energy is written as

$$T_t = \frac{1}{2}\int_0^L \rho S (\mathbf{r}')^2 ds,$$

where ρS and $\mathbf{r}'$ have the same meaning as in Eq.(10). The rotational energy is given as

$$T_r = \frac{1}{2}\int_0^L \rho \mathbb{K}^T \mathbb{I} \mathbb{K} ds,$$

where $\mathbb{K}$ is the curvature matrix, $\mathbb{K} = (q_0, q_1, q_2)^T$, $\mathbb{K}^T$ is the transposed matrix of $\mathbb{K}$, $\mathbb{I} = \begin{pmatrix} I_0 & & \\ & I_1 & \\ & & I_2 \end{pmatrix}$, it is the inertial tensor simplified as

$$I_0 = \frac{\pi a_1^3 a_2^3}{2(1+\sigma)(a_1^2 + a_2^2)}, I_1 = \frac{\pi}{4} a_1 a_2^3, \quad I_2 = \frac{\pi}{4} a_1^3 a_2,$$

where σ is the Poisson's ration (0.48 for hair), a_1 and a_2 are the horizontal and vertical radius length of ellipse cross section.

Since the rod of hair is inextensible, the potential energy V is of the bending and torsion deformation. It can be written as

$$V = \frac{1}{2}\int_0^L \mathbb{H}^T \mathbb{C}^H \mathbb{H} ds,$$

where $\mathbb{H} = (q_0 - q_0^0, q_1 - q_1^0, q_2 - q_2^0)^T$, $q_j^0 (j = 0, 1, 2)$ is the intrinsic bending and torsion of the hair rod, $\mathbb{H}^T$ is the transposed matrix of $\mathbb{H}$, $\mathbb{C}^H = \begin{pmatrix} EI_0 & & \\ & EI_1 & \\ & & EI_2 \end{pmatrix}$, $\mathbb{C}^H$ is the stiffness tensor, E is the Young's modulus, I_j $(j = 0, 1, 2)$ is the same as in matrix $\mathbb{I}$.

Just as the potential energy above, for this inextensible hair rod, we only consider the dissipative bending and torsion energy. The dissipation energy D can be given by

$$D = \frac{1}{2}\int_0^L \mu (\mathbb{K}')^T \mathbb{C}^{\mathbb{K}'} (\mathbb{K}') ds,$$

where $\mathbb{K}' = (q_0', q_1', q_2')^T$ is the hair curvature rate, $(\mathbb{K}')^T$ is the transposed matrix of $\mathbb{K}'$, $\mathbb{C}^{\mathbb{K}'}$ is equivalent to $\mathbb{C}^H$ in V, μ is the inter-hair frictional coefficient (0.1 in practice).

By plugging all terms into Eq.(9), we arrive at explicit equations of motion for the generalized coordinate $\mathbf{q}$. The final equation of motion for a helix is:

$$(\rho S \mathbb{M} + \Delta t \mu \mathbb{A} + \Delta t^2 \mathbb{A}) \frac{\Delta \mathbf{q}}{\Delta t} = \rho S \mathbb{M} \mathbf{q}' - \nu \mathbb{M} \mathbf{q}' \Delta t + \Delta t [(\mathbf{C} + \mathbf{Q}^{col}) + \mathbb{A}(\mathbf{q}^0 - \mathbf{q}) - \mathbb{B}\mathbf{q}]. \quad (11)$$

In Eq.(11), the matrix $\mathbb{M}$ is a dense symmetric matrix of size $3N \times 3N$, which depends nonlinearly on $\mathbf{q}$. The stiffness matrixes $\mathbb{A}$ and $\mathbb{B}$ are diagonal, are filled with bending and torsional stiffness of the helix, and have the same size $3N$. Δt is the time step for simulation, $\frac{\Delta \mathbf{q}}{\Delta t}$ is the curvature rate change of time, μ is the coefficient of friction among hair, $\mathbf{q}'$ is the derivative of $\mathbf{q}$ to t. $\mathbf{Q}^{col}$ corresponds to collision force. $\mathbf{C}$ collects all the other terms, including viscous and air drag dissipation. We solve this system of linear equations by conjugate gradient method.

Finally, we exploit the basic idea of simulating only a small set of guide hair strands and interpolating the motion of a full set of hair strands. Instead of interpolating an entire strand of a normal hair from guide hair strands, we propose to interpolate every normal hair particle from a subset of hair particles on guide hair strands. The interpolation weights for each hair particle are optimized by solving a linearly constrained least-square problem [40].

VII. RESULTS AND DISCUSSIONS

A. IMPLEMENTATION DETAILS

Our capture device is shown in Figure 2. To reduce sharp shadows, we place two LED panels at the top and bottom of hair respectively. We make a 3D calibration box and hang it in the upper part of the hairstyle to obtain valid information for calibration. We calibrate extrinsic parameters by ARTag [41] at different viewpoints. We use a super-helix model similar

FIGURE 3. Examples of our image-based hair modeling method applied to five datasets. For each, we show two views of the reference input images and the modeling results. From left to right are the input images and the modeling results at view 1, the input images and the modeling results at view 2. The number of hair in each datasets is 50K.

to [3] for hair simulation. For different hairstyles, we adjust the intrinsic simulation parameters (linear mass density and stiffness) to get plausible dynamic behavior. We use the same parameter values for a hairstyle throughout our experiment. Since our work is more related to styling than rendering, we render all figures and animations in this paper in real time with single scattering formulation [42] instead of multiple scattering [43], [44].

B. EXPERIMENTAL RESULTS

As shown in Figure 3, our hair modeling method is able to reconstruct different hairstyles. The first row is of black straight real hair. Although camera calibration and image matting are difficult for this hairstyle, our reconstructed results are relatively accurate and suitable for virtual characters. The last four rows are of wigs. The second row contains many wavy wisps that present a challenge to preserve structural details, while the third row illustrates a complicated hairstyle. Most of the curls in this hairstyle are constructed. The fourth and fifth rows illustrate long straight hairstyles with curved wisps at their bottom.

We validate our physics-based hair model on captured hairstyles. Experiments show that the model can generate dynamic features of hair. Figure 4 shows some simulation results driven by head moving or wind blowing. Please refer to the accompanied video for complete motion results. In addition to captured hairstyles, we also validate our method with simulation data. As shown in Figure 5, the physics-based model can generate detailed hair motion results driven by head motion or wind force. Please see the accompanied video for the complete simulation results.

C. DISCUSSIONS

1) COMPARISONS

We compare our image-based hair modeling method with the state-of-the-art structure-aware method [8]. As we can see from Figure 6, their method can preserve the exterior structural details of hairstyles. However, their method directly synthesizes strands from wisps, and results in unrealistic hair strands (e.g., abrupt hair in Figure 6(b)). In contrast to this, we generate a hair model from a hybrid orientation field, this can preserve the structural details of hairstyle (as shown in Figure 6(c)). We also compare our method with dynamic hair capture method [9]. They construct a orientation field using directed ribbons. The initial result could match most of the original hair. However, the surface of the hair model is rugged since the field is directly generated from directed ribbons (e.g., Figure 7(c)). They solve this problem by making the best of motion paths theory and EM-like optimization algorithm in dynamic hair capture. In our method, we present a hybrid orientation field to reconstruct a 3D hair model (e.g., Figure 7(b)). Compared with the method in [35] (e.g., Figure 7(d)), our method (e.g., Figure 7(b)) can preserve the exterior structural details of hair, especially at the tips of hairstyle. We achieve this through two aspects, on the one hand, we use the directed ribbons and Laplace equation for orientation diffusion instead of fractional anisotropy; on the other hand, we use the *directed hair ribbons* to preserve exterior structure of a hairstyle instead of strand-based optimization strategy, which is the most time-consuming part in [35].

Nextly, we compare our adaptive floating tangents fitting algorithm against the natural optimization [45] and the floating tangents method [38]. We applied these three algorithms on three hairstyles (short straight hairstyle, curly hairstyle, and long straight hairstyle) captured by our image-based

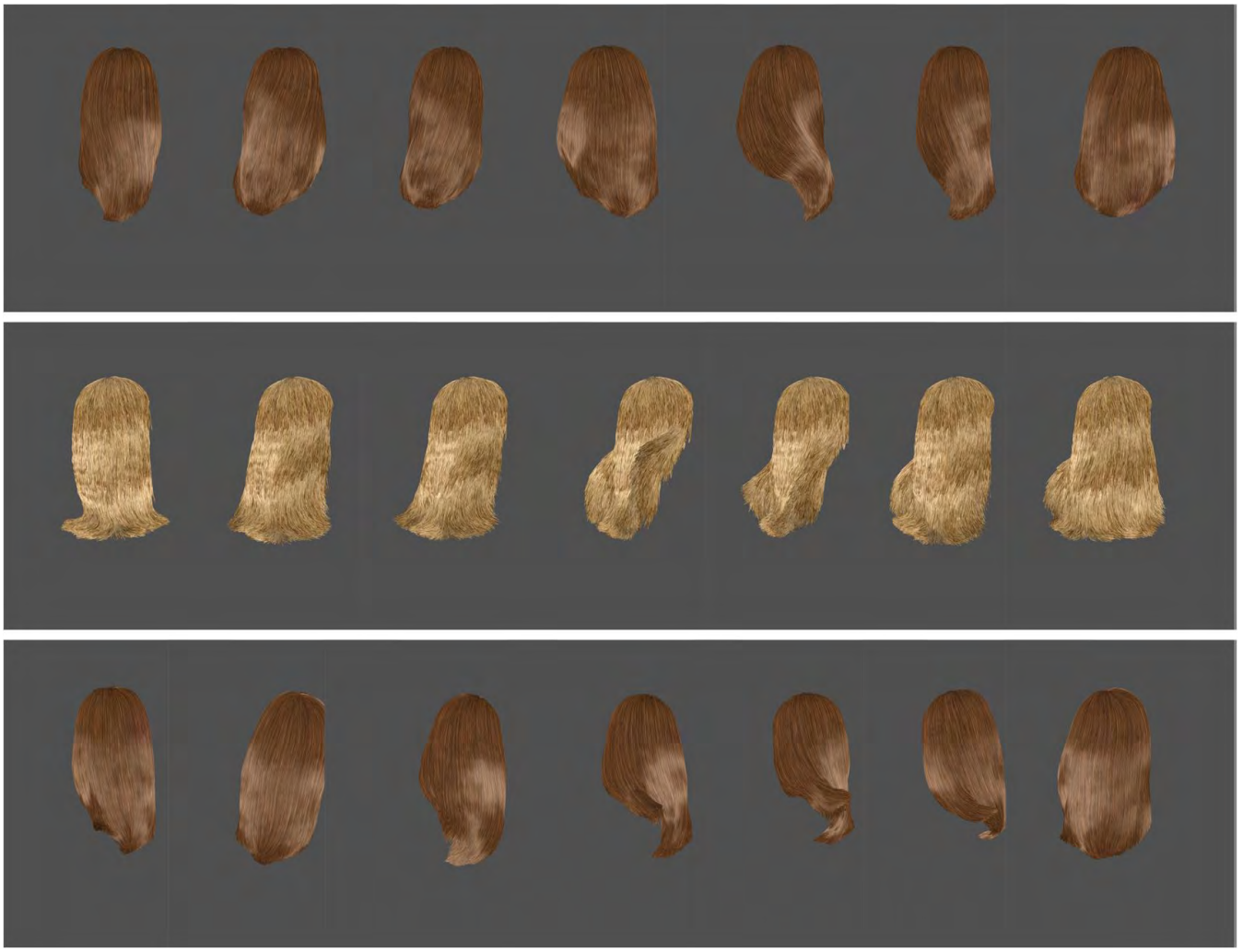

FIGURE 4. Simulation results generated by our method with captured hairstyles. Top row shows the head shaking of long straight hairstyle, middle row demonstrates the wind blowing of wavy hairstyle, and bottom row shows the head moving for long straight hairstyle. The number of hair for each hairstyle is 50K. See the accompanied video for more results.

hair modeling method. Each one of those hairstyles contains around 5K splines. The length of splines for each hairstyle are about 25cm, 40cm, and 60cm. In Figure 8, the helical elements applied to these three hairstyles for optimization method and floating tangents method are constant, with $N = 15$. In our adaptive method, the helical elements applied to these three hairstyles (from the first row to the last row in Figure 8) are variable, with $N = 14$, $N = 24$, *and* $N = 18$ for each hairstyle. As shown in Figure 8, the quality of the approximation with our adaptive floating tangents fitting is more better than other two methods, especially at complex part of these hairstyles. We display in Table. 2 the computation time of three approximation algorithms applied to three hairstyles in Figure 8. In contrast, the computation time of the optimization method is more difficult to predict as the complexity of the hair increases. However, our method can run at a constant speed, whatever the complexity of the input hairstyle is.

TABLE 2. Computation time in seconds of our adaptive floating tangents fitting algorithm compared to other approaches. The number of hair for each hairstyle is about 5K.

	Hairstyle A	Hairstyle B	Hairstyle C
Our method	2.4	2.5	2.5
Optimization	1.1	14.7	2.6
Floating tangents	3.1	4.8	4.5

2) PARAMETERS

We use the default set of parameters for all our experiments except α_s, α_i, α_d, and α_g in Eq. (1). These four parameters are dynamical weights which can be calculated in Sec. IV. We summarize important parameters in Table. 3 for easy loop-up.

3) TIMINGS

Our hair modeling method is mostly automatic except manually selecting the area of hair roots. It takes less than five

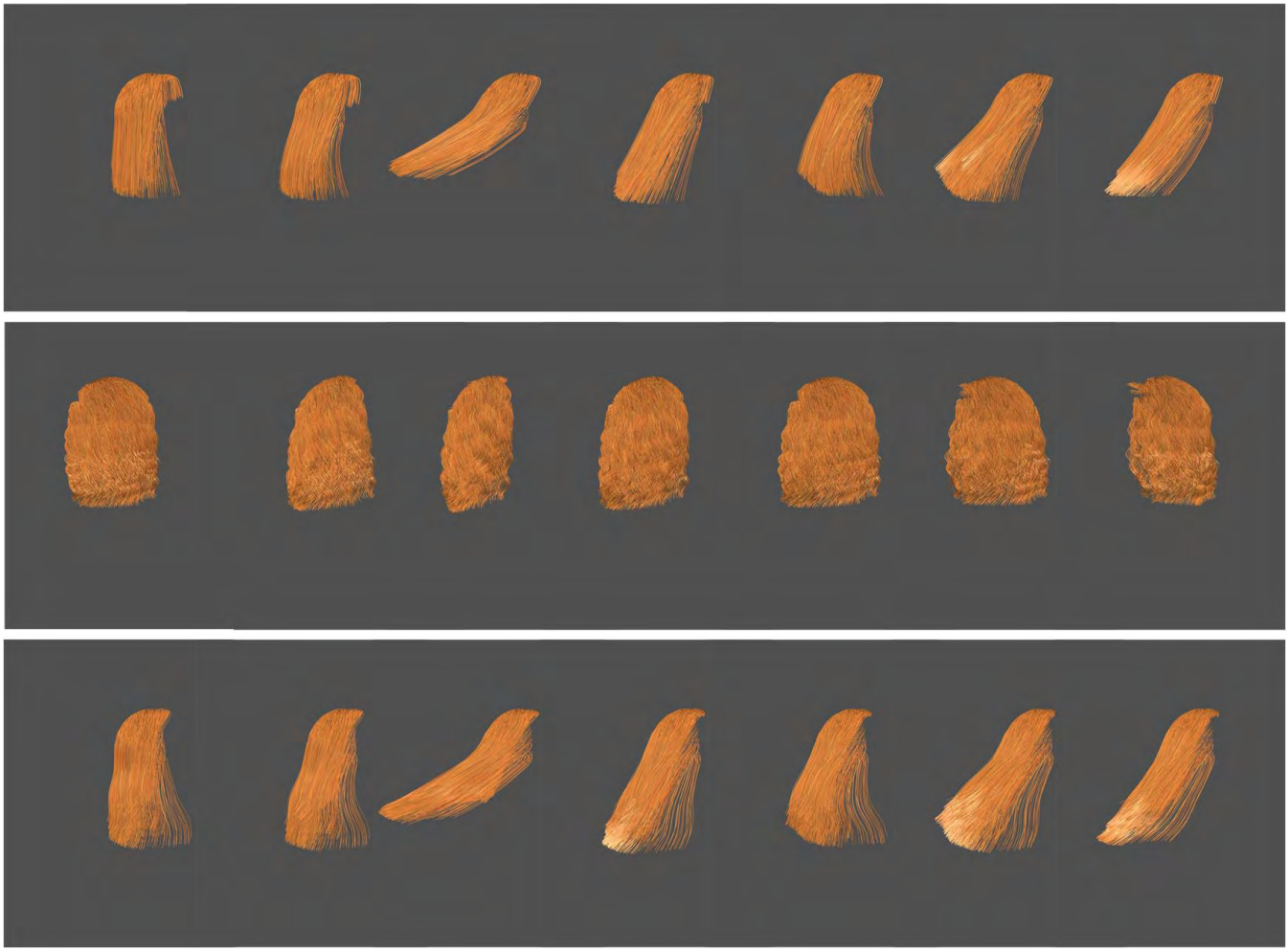

FIGURE 5. Simulation results generated by our method with simulation datas. Top row demonstrates the wind blowing of straight hairstyle, middle row shows the head shaking for curly hairstyle, and bottom row shows the wind blowing for long wavy hairstyle. The number of hair for each hairstyle is 10K. See the accompanied video for complete simulation results.

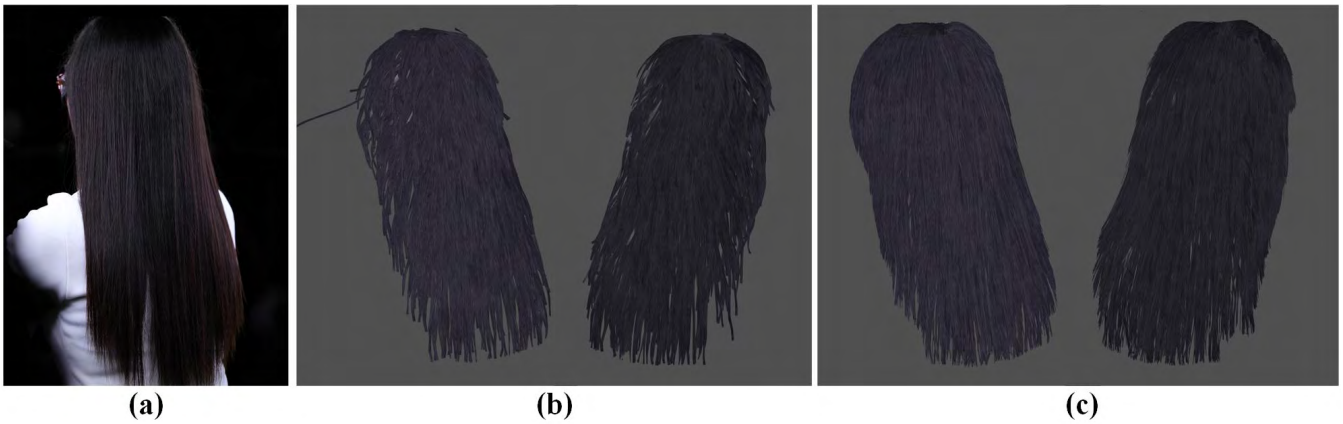

FIGURE 6. Comparison with structure-aware hair modeling method. From left to right: (a) reference image; (b) results of Luo *et al.* [8]; (c) our results. The number of hair in each result is 50K.

minutes for this manual operation. Timings were measured on a single threaded application running on an Intel i7 PC with 32G memory. For 38 input images, pretreatment before tracing directed 3D strand segments takes about thirty minutes. The computation for hybrid orientation field takes no more than five minutes. The final constructing a

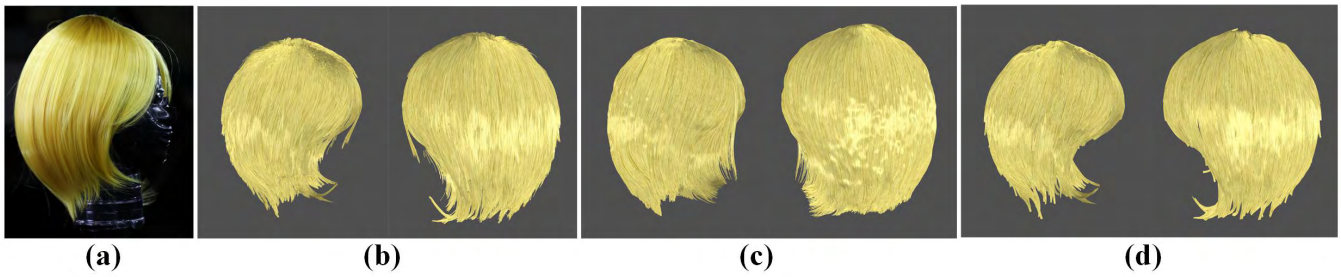

FIGURE 7. Comparison with other hair modeling methods. (a) reference image; results reconstructed by (b) our method, (c) Xu *et al.* [9], and (d) Bao and Qi [35]. The number of hair in each result is 50K.

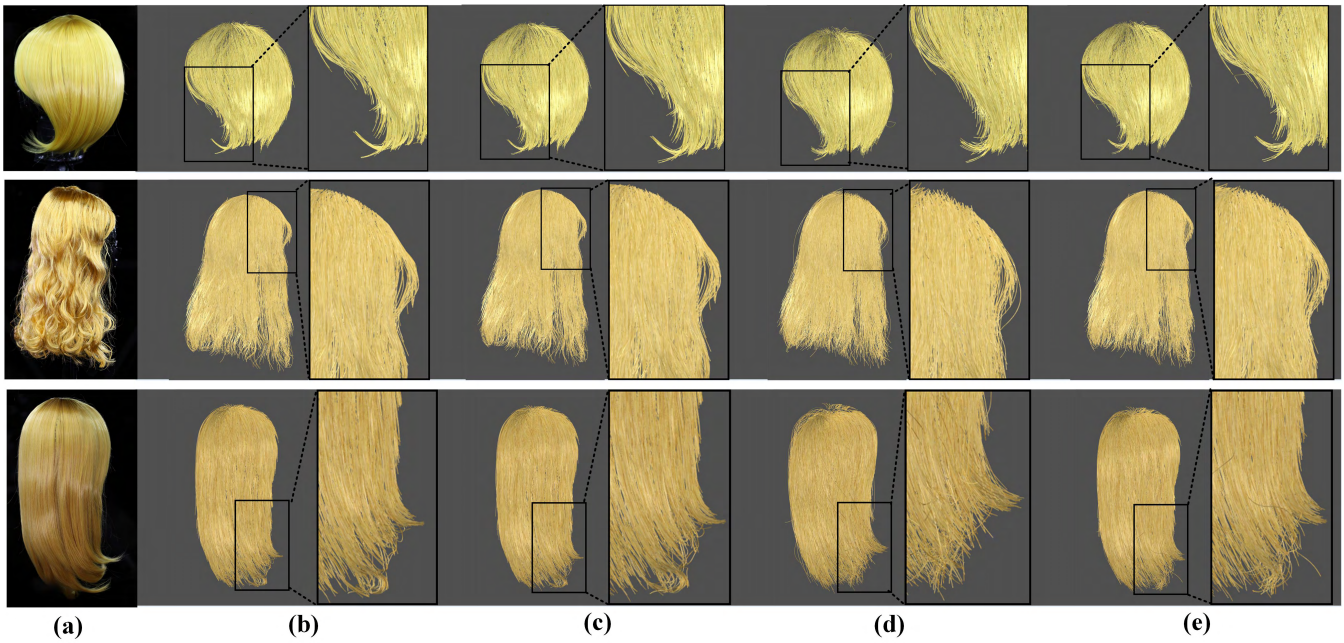

FIGURE 8. The three hairstyles A, B, and C(corresponding to short straight hairstyle, curly hairstyle, and long straight hairstyle from the first row to the last row) and the approximation results. From left to right: (a) backgrounds; (b) the input hairstyles; (c) results produced by our adaptive floating tangents fitting method, (d) optimization method [45], and (e) floating tangents method [38]. The number of hair for each hairstyle is about 5K.

TABLE 3. Parameter values used in our experiments.

I_{bound}	N_{min}	N_{max}	L_{min}	L_{max}	Input images
0.1	3	25	5cm	80cm	38
In Sec.IV	In Sec.V-A				In Sec.III

3D hair model takes about 2 minutes. Compared with Bao and Qi [35](about 100 minutes), our method only takes about 40 minutes to reconstruct a hairstyle.

4) LIMITATIONS

Although our method can reconstruct most of the hairstyles, the representation form of orientation field prevent our method from reconstructing extremely complex hairstyles (e.g., the Marilyn Monroe hairstyle). We cannot represent the direction of this hairstyle on a regular grid. We use a reduced model to accelerate hair simulation. Although our approach yielded satisfying results in our tests, it may be a poor approximation if external forces severely alter the balance of hair simulation.

VIII. CONCLUSION

We have introduced a novel approach for hair simulation from captured input images. We convert a hair geometry model into a physics-based hair model and simulate hair features. By using the direction and structural characteristics of directed 3D strand segments, we are able to generate a structural details preserving hybrid orientation field, and thereby to preserve exterior structural details of a hairstyle. We convert the reconstructed realistic 3D hair geometry model into a physics-based hair model. Each hair strand is approximated with G^1 piecewise helices by our adaptive floating tangents fitting algorithm. Parameters of these helices can be computed by this algorithm. Then we get a

physics-based hair model. Having calculated a corresponding static equilibrium configuration under external forces, we simulate dynamic hair features by this model to verify the effectiveness of our method. In the future we would like to further enhance our method to cover a broader range of hairstyle.

ACKNOWLEDGMENT

The authors would like to thank the anonymous reviewers for their valuable comments and helpful suggestions.

REFERENCES

[1] Y. Wei, E. Ofek, L. Quan, and H.-Y. Shum, "Modeling hair from multiple views," *ACM Trans. Graph.*, vol. 24, no. 3, pp. 816–820, 2005.

[2] S. Paris *et al.*, "Hair photobooth: geometric and photometric acquisition of real hairstyles," *ACM Trans. Graph.*, vol. 27, no. 3, pp. 30:1–30:9, 2008.

[3] F. Bertails, B. Audoly, M.-P. Cani, B. Querleux, F. Leroy, and J.-L. Lévêque, "Super-helices for predicting the dynamics of natural hair," *ACM Trans. Graph.*, vol. 25, no. 3, pp. 1180–1187, 2006.

[4] K. Ward, F. Bertails, T. Y. Kim, S. R. Marschner, M. P. Cani, and M. C. Lin, "A survey on hair modeling: Styling, simulation, and rendering," *IEEE Trans. Vis. Comput. Graphics*, vol. 13, no. 2, pp. 213–234, Mar. 2007.

[5] T. Yamaguchi, B. Wilburn, and E. Ofek, "Video-based modeling of dynamic hair," in *Advances in Image and Video Technology*. Berlin, Germany: Springer, 2009, pp. 585–596.

[6] T. L. Herrera, A. Zinke, and A. Weber, "Lighting hair from the inside: A thermal approach to hair reconstruction," *ACM Trans. Graph.*, vol. 31, no. 6, pp. 146:1–146:9, 2012.

[7] T. Beeler *et al.*, "Coupled 3D reconstruction of sparse facial hair and skin," *ACM Trans. Graph.*, vol. 31, no. 4, p. 117, 2012.

[8] L. Luo, H. Li, and S. Rusinkiewicz, "Structure-aware hair capture," *ACM Trans. Graph.*, vol. 32, no. 4, pp. 76:1–76:11, 2013.

[9] Z. Xu, H.-T. Wu, L. Wang, C. Zheng, X. Tong, and Y. Qi, "Dynamic hair capture using spacetime optimization," *ACM Trans. Graph.*, vol. 33, no. 6, pp. 224:1–224:11, Nov. 2014.

[10] X. Yu, Z. Yu, X. Chen, and J. Yu, "A hybrid image-cad based system for modeling realistic hairstyles," in *Proc. 18th Meet. ACM SIGGRAPH Symp. Interact. 3D Graph. Games*, 2014, pp. 63–70.

[11] N. Bonneel, S. Paris, M. Van De Panne, F. Durand, and G. Drettakis, "Single photo estimation of hair appearance," *Comput. Graph. Forum*, vol. 28, no. 4, pp. 1171–1180, 2009.

[12] M. Chai, L. Wang, Y. Weng, Y. Yu, B. Guo, and K. Zhou, "Single-view hair modeling for portrait manipulation," *ACM Trans. Graph.*, vol. 31, no. 4, pp. 116:1–116:8, 2012.

[13] J. I. Echevarria, D. Bradley, D. Gutierrez, and T. Beeler, "Capturing and stylizing hair for 3D fabrication," *ACM Trans. Graph.*, vol. 33, no. 4, p. 125, 2014.

[14] L. Hu, C. Ma, L. Luo, and H. Li, "Single-view hair modeling using a hairstyle database," *ACM Trans. Graph.*, vol. 34, no. 4, p. 125, Aug. 2015.

[15] M. Chai, L. Luo, K. Sunkavalli, N. Carr, S. Hadap, and K. Zhou, "High-quality hair modeling from a single portrait photo," *ACM Trans. Graph.*, vol. 34, no. 6, p. 204, 2015.

[16] M. Chai, T. Shao, H. Wu, Y. Weng, and K. Zhou, "AutoHair: Fully automatic hair modeling from a single image," *ACM Trans. Graph.*, vol. 35, no. 4, p. 116, 2016.

[17] R. E. Rosenblum, W. E. Carlson, and E. Tripp, III, "Simulating the structure and dynamics of human hair: Modelling, rendering and animation," *Comput. Animation Virtual Worlds*, vol. 2, no. 4, pp. 141–148, 1991.

[18] K.-I. Anjyo, Y. Usami, and T. Kurihara, "A simple method for extracting the natural beauty of hair," *ACM SIGGRAPH Comput. Graph.*, vol. 26, no. 2, pp. 111–120, 1992.

[19] A. Selle, M. Lentine, and R. Fedkiw, "A mass spring model for hair simulation," *ACM Trans. Graph.*, vol. 27, no. 3, p. 64, 2008.

[20] A. McAdams, A. Selle, K. Ward, E. Sifakis, and J. Teran, "Detail preserving continuum simulation of straight hair," *ACM Trans. Graph.*, vol. 28, no. 3, p. 62, 2009.

[21] H. Iben, M. Meyer, L. Petrovic, O. Soares, J. Anderson, and A. Witkin, "Artistic simulation of curly hair," in *Proc. 12th ACM SIGGRAPH/Eurograph. Symp. Comput. Animation*, 2013, pp. 63–71.

[22] G. Gornowicz and S. Borac, "Efficient and stable approach to elasticity and collisions for hair animation," in *Proc. Symp. Digit. Prod.*, 2015, pp. 41–49.

[23] D. M. Kaufman, R. Tamstorf, B. Smith, J.-M. Aubry, and E. Grinspun, "Adaptive nonlinearity for collisions in complex rod assemblies," *ACM Trans. Graph.*, vol. 33, no. 4, p. 123, 2014.

[24] M. Bergou, B. Audoly, E. Vouga, M. Wardetzky, and E. Grinspun, "Discrete viscous threads," *ACM Trans. Graph.*, vol. 29, no. 4, p. 116, 2010.

[25] G. Daviet, F. Bertails-Descoubes, and L. Boissieux, "A hybrid iterative solver for robustly capturing coulomb friction in hair dynamics," *ACM Trans. Graph.*, vol. 30, no. 6, p. 139, 2011.

[26] M. Chai, C. Zheng, and K. Zhou, "Adaptive skinning for interactive hair-solid simulation," *IEEE Trans. Vis. Comput. Graphics*, vol. 23, no. 7, pp. 1725–1738, Jul. 2017.

[27] F. Yun, H. T. Maia, C. Batty, C. Zheng, and E. Grinspun, "A multi-scale model for simulating liquid-hair interactions," *ACM Trans. Graph.*, vol. 36, no. 4, pp. 56:1–56:17, Jul. 2017.

[28] S. Hadap, "Oriented strands: Dynamics of stiff multi-body system," in *Proc. ACM SIGGRAPH/Eurograph. Symp. Comput. Animation*, 2006, pp. 91–100.

[29] A. Derouet-Jourdan, F. Bertails-Descoubes, and J. Thollot, "Stable inverse dynamic curves," *ACM Trans. Graph.*, vol. 29, no. 6, p. 137, 2010.

[30] C. D. Twigg and Z. Kačić-Alesić, "Optimization for sag-free simulations," in *Proc. ACM SIGGRAPH/Eurograph. Symp. Comput. Animation*, 2011, pp. 225–236.

[31] S. Hadap and N. Magnenat-Thalmann, "Modeling dynamic hair as a continuum," *Comput. Graph. Forum*, vol. 20, no. 3, pp. 329–338, 2001.

[32] Y. Bando, B.-Y. Chen, and T. Nishita, "Animating hair with loosely connected particles," *Comput. Graph. Forum*, vol. 22, no. 3, pp. 411–418, 2003.

[33] Q. Chen, D. Li, and C. K. Tang, "KNN matting," *IEEE Trans. Pattern Anal. Mach. Intell.*, vol. 35, no. 9, pp. 2175–2188, Sep. 2013.

[34] Y. Furukawa and J. Ponce, "Accurate, dense, and robust multiview stereopsis," *IEEE Trans. Pattern Anal. Mach. Intell.*, vol. 32, no. 8, pp. 1362–1376, Aug. 2008.

[35] Y. Bao and Y. Qi, "Realistic hair modeling from a hybrid orientation field," *Vis. Comput.*, vol. 32, nos. 6–8, pp. 729–738, 2016.

[36] Y. Lu, K. Shi, J. Yong, H. Gu, and H. Song, "A B-spline curve extension algorithm," *Sci. China Inf. Sci.*, vol. 59, no. 3, p. 32103, 2016.

[37] S. Ghosh, "Geometric approximation of curves and singularities of secant maps. A differential geometric approach," Ph.D. dissertation, Groningen Graduate School Sci., Univ. Groningen, Groningen, The Netherlands, 2010.

[38] A. Derouet-Jourdan, F. Bertails-Descoubes, and J. Thollot, "Floating tangents for approximating spatial curves with G1 piecewise helices," *Comput. Aided Geometric Des.*, vol. 30, no. 5, pp. 490–520, 2013.

[39] A. Derouet-Jourdan, F. Bertails-Descoubes, G. Daviet, and J. Thollot, "Inverse dynamic hair modeling with frictional contact," *ACM Trans. Graph.*, vol. 32, no. 6, p. 159, 2013.

[40] M. Chai, C. Zheng, and K. Zhou, "A reduced model for interactive hairs," *ACM Trans. Graph.*, vol. 33, no. 4, p. 124, 2014.

[41] M. Fiala, "ARTag, a fiducial marker system using digital techniques," in *Proc. IEEE Comput. Soc. Conf. Comput. Vis. Pattern Recognit. (CVPR)*, vol. 2. Jun. 2005, pp. 590–596.

[42] S. R. Marschner, H. W. Jensen, M. Cammarano, S. Worley, and P. Hanrahan, "Light scattering from human hair fibers," *ACM Trans. Graph.*, vol. 22, no. 3, pp. 780–791, 2003.

[43] L.-Q. Yan, C.-W. Tseng, H. W. Jensen, and R. Ramamoorthi, "Physically-accurate fur reflectance: Modeling, measurement and rendering," *ACM Trans. Graph.*, vol. 34, no. 6, p. 185, 2015.

[44] E. d'Eon, S. Marschner, and J. Hanika, "Importance sampling for physically-based hair fiber models," in *Proc. SIGGRAPH Asia Tech. Briefs*, 2013, pp. 1–4.

[45] A. Derouet-Jourdan, F. Bertails-Descoubes, and J. Thollot, "3D inverse dynamic modeling of strands," in *Proc. ACM SIGGRAPH Posters*, 2011, p. 55.

YONGTANG BAO received the B.S. and M.S. degrees in computer science from the China University of Petroleum. He is currently pursuing the Ph.D. degree with the State Key Laboratory of Virtual Reality Technology and Systems, Beihang University. His research interests include virtual reality, image-based modeling, and geometric modeling.

YUE QI (M'09) received the Ph.D. degree from the National University of Defense Technology. He then joined Beihang University in 2001. He is currently a Professor with the State Key Laboratory of Virtual Reality Technology and Systems, Beihang University. His research interests include virtual reality, augmented reality, and computer graphics. He is a member of the ACM.